Histogram Partitioning Algorithms for Adaptive and Autonomous Threshold Estimation in Cognitive Radio based Industrial Wireless Sensor Networks

A. J. Onumanyi*[1], A. M. Abu-Mahfouz[2,1] and G. P. Hancke[3,1]

1Department of Electrical, Electronic and Computer Engineering, University of Pretoria, Pretoria, South Africa
2Council for Scientific and Industrial Research, Pretoria, South Africa
3Department of Computer Science, City University of Hong Kong, Hong Kong, China

*Correspondence: A. J. Onumanyi, Email: adeiza1@futminna.edu.ng

Summary

Modern energy detectors typically use adaptive threshold estimation algorithms to improve signal detection in cognitive radio–based industrial wireless sensor networks (CR-IWSNs). However, a number of adaptive threshold estimation algorithms often perform poorly under noise uncertainty conditions since they are typically unable to auto-adapt their parameter values per changing spectra conditions. Consequently, in this paper, we have developed two new algorithms to accurately and autonomously estimate threshold values in CR-IWSNs under dynamic spectra conditions. The first algorithm is a parametric-based technique termed the histogram partitioning algorithm, whereas the second algorithm is a fully autonomous variant termed the mean-based histogram partitioning algorithm. We have evaluated and compared both algorithms with some well-known methods under different CR sensing conditions. Our findings indicate that both algorithms maintained over 90% probability of detection in both narrow and wideband sensing conditions and less than 10% probability of false alarm under noise-only conditions. Both algorithms are quick and highly scalable with a time complexity of O(V), where V is the total number of input samples. The simplicity, effectiveness, and viability of both algorithms make them typically suited for use in CR-IWSN applications.

Keywords: Cognitive Radio, Industrial Wireless Sensor Networks, Parametric, Signal detection, Threshold

1. Introduction

Most industrial wireless sensor networks (IWSNs) are designed to operate in the Industrial, Scientific, and Medical (ISM) bands. However, because ISM bands are now becoming highly congested, recent IWSN designs now adopt cognitive radio (CR) technologies in order to improve communication and spectra efficiency over vacant licensed bands[1,2]. For example, authors in[3] have developed an interesting prototype of a CR based industrial process field-bus to improve communication in automated factory processes. Successful designs such as in[3] affirm the viability of CR for use within different IWSN based applications, for example in cyber-physical systems (CPS)[4,5], low power wide area networks (LPWANs)[6], smart grids[7,8], tele-intensive care units[9], in smart metering, and smart city applications[10,11].

However, in order to be effective, the challenge of spectrum sensing (SS) must be considered in the design of CR based IWSN systems since these systems use SS to determine whether a licensed band is free or not to communicate opportunistically. Consequently, a number of works typically employ the Energy Detector (ED) for purpose of SS in CR-IWSN systems because the ED is the fastest, simplest, cheapest,

and least energy-consuming detector, which makes it suited for resource-constrained IWSNs[2]. Other detectors such as the Cyclostationary Detector, Eigenvalue, Covariance, Prediction, and Evolutionary-based detectors[12,13,14] are not suited for CR-IWSNs applications because they are complex, introduce long sensing delays, are dependent on the knowledge of the Primary User (PU) signal, and typically require higher energy rates to operate[15,16,17].

Nevertheless, EDs are generally susceptible to errors such as false alarms and misdetections, which often arise under noise uncertainty conditions in low signal-to-noise ratio (SNR) regimes (< 3dB)[18]. To minimize these errors, modern EDs use adaptive threshold estimation algorithms (ATAs) to estimate useful thresholds without prior knowledge of the noise level in the spectra[19]. Adapting threshold values under noise uncertainty conditions describes the adaptation problem. Furthermore, ATAs may need to adjust their parameter values automatically to improve performance under dynamic spectra conditions and we refer to this requirement for auto-tuning as the autonomous problem. Methods that address the autonomous problem are referred to as autonomous ATAs (AATAs). Henceforth, we shall refer to non-autonomous ATAs simply as *adaptive-only* methods while AATAs will be called autonomous methods.

Concerning the autonomous problem, only very few notable methods exist, which are typically non-parametric methods. By being non-parametric, these AATAs are notably more robust than their *adaptive-only* counterparts[20]. This is because most *adaptive-only* methods typically assume that the sample population being sensed is known, but when this assumption is wrong, they would typically fail. Consequently, researchers seek continually to develop better effective AATAs for use in CR. Thus, the quest to develop simple, quick, and highly scalable algorithms suited for resource-limited CR-IWSNs motivated the new methods described in this paper.

Consequently, in this paper, we have proposed two threshold estimation algorithms for signal detection in EDs suited for CR-IWSNs. First, we have introduced an *adaptive-only* method termed the Histogram Partitioning Algorithm (HPA) and then an autonomous method termed the Mean HPA (MHPA). A few realistic application scenarios where our algorithms can be used include for opportunistic and reliable communication in smart factories and industries (driven under Industrie 4.0), and for reliable communication between cyber-physical systems. Essentially, sensors that measure specific physical parameters such as temperature, humidity, smoke, e.t.c in an industrial environment can be equipped with our CR-based algorithms. Then, these CR-based sensors will use our algorithms to accurately and autonomously detect free bands in order to communicate these measured parameters reliably to a central processing unit. The central processing unit can then activate some specific actuators in order to execute a corresponding action within the factory. We have developed and extensively tested both algorithms under different spectra conditions. Our findings suggest that the following contributions are tenable:

1. Two new adaptive methods namely, the HPA and MHPA have been developed to estimate useful thresholds in CR-based applications without prior knowledge of the noise level or the power or frequency of the PU signal in the band.

2. Both algorithms are independent of the size of the band being sensed making them effective methods for both narrow and wideband sensing in CR.

3. The MHPA is an effective and fully autonomous method that performs better than some existing autonomous and state-of-the-art *adaptive-only* methods. Hence, we consider the MHPA suited for fully blind spectrum sensing in CR. Since IWSNs typically require spartially distributed energy-constrained, self-configuring and self-aware sensor nodes, our MHPA being an autonomous method will be highly suited for such IWSN applications.

4. Both algorithms maintain a low probability of false alarm, P_{FA}, particularly under low SNR regimes. They conform effectively to the IEEE 802.22 standard, which requires a detector to maintain a probability of detection, P_D, higher than 90 %, and a P_{FA} rate less than 10 %[21].

5. Both algorithms have a time complexity of $O(V)$, where V is the total number of sensed samples, thus implying that they are quick and highly scalable algorithms. They are considered useful methods for resource constrained CR-IWSNs.

2. Related work

We motivate two main issues in our discussion of the related work: first, we identify some state-of-the-art *adaptive-only* methods, which are closely related to the class of autonomous methods suited for resource-limited IWSN applications. Second, we provide motivation for the study of autonomous methods, including the need to develop better autonomous methods.

To identify related *adaptive-only* methods, we considered only global-based methods because they are notably better suited for CR applications (kindly see[22] for details). Furthermore, we have considered only methods with minimal parameter sets (that is, two or fewer parameters) in order to be viable for resource constrained CR-IWSN applications. This is implied by selecting *adaptive-only* methods that are simple and considered relatively close to the class of autonomous methods. Choosing such methods facilitates fairer comparative analyses between *adaptive-only* and autonomous methods, which we considered in this paper. In this regard and to the best of our knowledge, the comparison of both *adaptive-only* and autonomous methods forms a notable difference between our study and other studies of threshold algorithms in the literature.

Consequently, some classic *adaptive-only* methods with two or fewer parameters are noted in[23,24,25,26]. These state-of- the-art algorithms are simple, close to being autonomous, and easy to develop. When deployed, they maintain the simplicity and fast sensing capability of the ED making them viable algorithms for CR based IWSNs. Examples of these algorithms include the Recursive One-sided Hypothesis Testing (ROHT) algorithm[23,24], the First Order Statistical Technique[25], the Maximum Normal Fit[26] (which is a modification of the ROHT) and the Forward Consecutive Mean Excision (FCME) algorithm[27]. Some other *adaptive-only* methods found in[28,29,30,31,32,33] typically depend on larger parameter sets. Though often effective, however, by being too highly parameterized, these algorithms are considered unrelated to our study.

Following the above, we motivate our concern for AATAs. Usually, most *adaptive-only* methods are characterized notably by fixed sets of parameters, which are typically defined before use. In contrast, autonomous methods (AATAs) differ because their parameters are not fixed and can either increase or even decrease automatically based on the input dataset collected per time[34]. In rare but well-known cases, existing AATAs are even parameter-less (the algorithm automatically controls the parameters), for example, the Otsu's method used in[23,24] and the modified Otsu's method in[20]. Furthermore, AATAs do not make assumptions about the sample distribution being sensed as obtained in most *adaptive-only* methods. Thus, they are better applied in unpredictable and dynamic sensing conditions found in CR based applications. For this reason, autonomous methods are favorably motivated for use in CR-IWSNs.

In this regard, we propose two new methods that differ from existing approaches. In particular, our HPA differs from existing *adaptive-only* methods following the introduction of an entirely new histogram bifurcation approach along with a new model to control the algorithm's P_{FA} rate. Also, our proposed MHPA differs from existing AATAs based on the mean of the histogram samples introduced in order to separate noise from signal samples. Our proposed methods do not only differ from previous approaches, but they are as well useful based on the positive simulation and empirical results obtained in this paper.

3. Proposed Algorithms

In this section, we describe the detection system in which our proposed algorithms are deployed. Next, we present our proposed algorithms and then analyze their time complexity. A summary of the symbols used in this paper and their meanings are presented in Table 1.

Table 1. Symbols used and their meanings

Symbol	Meaning
P_{FA}	Probability of false alarm
P_D	Probability of detection
γ	Threshold
n	Time sample index
N	Total number of time domain samples
T	Sensing period
f_s	Sampling frequency
V	Number of frequency domain samples
k	Frequency sample index
$Y(k)$	Power Spectral Density
$y(n)$	Time domain received signal
β	*Descent* parameter
i	bin index
C_i	Sample counts per bin
B_i	Bin center value
M	Number of bins
C_i^{filt}	Smoothened counts per bin
Λ	Noise peak index
B_Λ	Mean noise value
ω	Smoothing window size
ρ	Counter

3.1. The Detection System

In our design, we have considered the ED as situated at the frontend of a typical CR based industrial wireless sensor node deployed to sense and communicate in an industrial wireless network environment. Typical ED designs can be found in[16]. Thus, in order to initiate communication, the sensor node uses the ED to sense free channels. Here, the ED uses an estimated threshold value γ to determine whether a specific channel is vacant or occupied in order to communicate opportunistically. The case H_0 is declared if the channel energy is less than or

equal to γ, which indicates that the spectra contains only noise samples; while the case H_1 is declared if the channel energy is greater than γ, which indicates that the spectra contains signal-plus-noise samples. These cases (hypotheses) are statistically described in the time domain as:

$$H_0 \ : \ y(n) = w(n), \quad n = 1, 2, ..., N \tag{1}$$

$$H_1 \ : \ y(n) = h(n)x(n) + w(n), \quad n = 1, 2, ..., N \tag{2}$$

where n is the time sample index, N is the total number of time domain input samples, $h(n)$ is the channel impulse response function, $x(n)$ is the transmitted signal, $w(n)$ is modeled as Additive White Gaussian Noise (AWGN). The output $y(n)$ is the received sampled signal at the frontend of an ED and we obtain N as $N = T \times f_s$ where T is the total sensing period and f_s is the sampling frequency. Furthermore, we know that a new input length V is required to compute the Fast Fourier Transformation (FFT) of $y(n)$, where V is the next power of 2 from the original signal length, N. This new length usually pads the signal with trailing zeros to improve the FFT's performance. Thus, we compute V as

$$V = 2^{\lceil \log_2(T f_S - 1) \rceil} \tag{3}$$

We have provided in the Appendix a short derivation of equation (3). Consequently, the ED estimates the Power Spectral Density (PSD) using

$$Y(k) = \left| \sum_{n=1}^{V-1} y(n) \exp\left(-j \frac{2\pi}{V} nk\right) \right|^2, \quad k = 1, 2, ..., V \tag{4}$$

where k is the frequency sample index. Each PSD sample $k = 1, 2...V$ is compared to γ to determine whether the channels k are free H_0 or not H_1. Thus, the performance of the ED depends typically on how accurately γ can be estimated. Consequently, estimating accurate γ values becomes essential to the overall success of CR-IWSNs. Thus, we shall describe in the next subsection our proposed algorithms considered to estimate accurate γ values.

3.2. The Histogram Partitioning Algorithms

The Histogram Partitioning Algorithm (HPA) and the Mean HPA (HPA) are simple and effective methods designed here to adapt the threshold of an ED. To achieve this, a sample histogram is used as a viable tool to separate effectively the multimodal distributions of an input signal. Consider the sketch of a typical histogram in Figure 1 showing the noise spread collocated between P_1 and P_3 (see red colour in Figure 1), and the signal spread at higher energy values (see green colour in Figure 1). The HPA effectively locates P_3, which corresponds to a useful threshold γ required to separate the noise from signal samples. In the low SNR case, where the signal

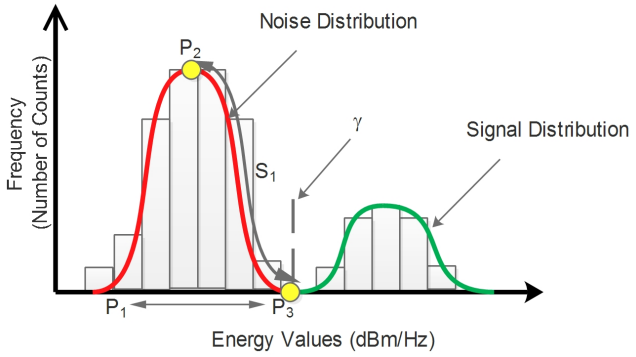

Figure 1. A typical Histogram demonstrating the HPA principle

distribution merges with the noise spread, the point P_3 corresponds to the minimum point along the negative slope of the noise distribution, S_1.

The HPA estimates the mean of the noise floor by locating the peak P_2 in the distribution (Figure 1) following a search of the histogram bin values. Any efficient peak-finding algorithm can be used to search for P_2. We note that P_2 corresponds typically to the mean noise floor (or noise mode) since more zero-crossing samples may exist in the noise than in the signal set. This assumption is valid for highly occupied bands, as our findings will demonstrate in Section 4. Furthermore, the HPA estimates a threshold factor (termed the *descent* parameter) as follows:

$$\beta = V \times P_{FA} \tag{5}$$

where V is the sample length computed in equation (3), and P_{FA} is the target false alarm rate specified by the user. Here, β corresponds to the frequency value (number of counts) obtained along the *ordinate* of the histogram (see Figure 1). In this case, β is found by searching through the values along S_1 beginning from P_2 towards P_3. Once obtained, β determines the stopping point along S_1, which corresponds to a useful γ obtained along the *abscissa*. Choosing small values leads to higher γ values and lower P_{FA} rates, and vice-versa. This relationship is well known between threshold values and their associated P_D and P_{FA} rates[35]. Based on the above explanation, we provide a detailed description of the HPA and the MHPA below with a summary provided in Algorithm 1. The HPA is distinguished from the MHPA in step 7 of Algorithm 1. Detailed description and justifications are provided as follows:

Step 1: The input signal, $y(n)$, $n = 1, 2, ...V$, is acquired via the ED and the PSD of the input signal is computed as $Y(k)$, $k = 1, 2, ..., V$, using equation (4). The PSD set $Y(k)$ has dimension V, which corresponds to the number of samples acquired over a single sweep of a specified band. Thus, each sample in $Y(k)$ corresponds to the energy of the signal in each frequency bin (channel).

Algorithm 1 The HPA/MHPA Algorithm

1: Compute the PSD of the input signal as $Y(k), k = 1, 2, ..., V$, using equation (4)
2: Compute the number of bins, M, using equation (6)
3: Compute the histogram of $Y(k)$
4: Smooth the counts C_i^{filt}, $i = 1, 2, ..., M - \omega + 1$ obtained from the histogram using a window size,ω
5: Find the highest peak, Λ, in the set C_i^{filt},
6: Find the bin centre value B_Λ corresponding to the highest peak, Λ
7: Compute the descent parameter β. This step differentiates the HPA from the MHPA
8: Initialize counter $\rho = \Lambda$
9: **if** $B_\Lambda < \max_{i \in M} \{B_i\}$ **then**
10: **while** $\rho = M$ **do**
11: $\rho = \rho + 1$
12: **if** $C_i^{filt} < \beta$ **then**
13: $\theta = \rho$
14: $\rho = M + 1$
15: **end if**
16: **end while**
17: **end if**
18: $\gamma = B_\theta$

Step 2: The number of bins, M, used to construct the histogram of the sample set is obtained using Doane's formula given as[36]:

$$M = 1 + \log_2(V) + \log_2\left(1 + \frac{|g_1|}{\sigma_{g_1}}\right) \tag{6}$$

where V is the total number of samples (obtained using equation (3)), g_1 is the estimated 3rd-moment (skewness) of the distribution and

$$\sigma_{g_1} = \sqrt{\frac{6(V-2)}{(V+1)(V+3)}} \tag{7}$$

We considered Doane's formula because it is simple and requires fewer computations than other known methods. It is also well suited for cases of non-normal distributions, which are obtained readily in CR networks.

Step 3: The histogram of $Y(k)$, $k = 1, 2, ..., V$ is computed using equation (8). The set of the sample counts per bin C_i, $i = 1, 2, ..., M$ and the set of the bin center values, B_i, $i = 1, 2, ..., V$ are obtained from the histogram of $Y(k)$. This histogram function is represented as

$$\left(C_i, B_i\right) = F_D\left(Y(k), M\right), \quad for\ D = 1 \tag{8}$$

where $D = 1$ stands for the case of a one dimensional (vector-based) dataset, and $F_D(\cdot)$ represents the normal histogram function. In this case, an effective method such as the Greedy Batch Dynamic Programming (GDY-BDP) method[37] can be used to compute the histogram.

Step 4: The samples C_i, $i = 1, 2, ..., M$ are smoothened using a moving average function with a window size, ω. This produces a smoother continuous histogram required to improve the estimated threshold value. The smoothening process is achieved using

$$C_i^{filt} = \frac{1}{\omega} \sum_{a=1}^{i+\omega-1} C_a, \quad i = 1, 2, ..., M - \omega + 1 \tag{9}$$

where C_i^{filt}, $i = 1, 2, ..., M - \omega + 1$ is the set of smoothened sample counts per bin, which closely approximates a PDF.

Step 5: The HPA searches C_i^{filt} in order to find the largest value denoted as C_Λ^{filt}, where Λ is the index of the largest value (corresponding to the noise peak index). This operation is obtained as $\left|C_\Lambda^{filt}, \Lambda\right| = \max\left\{C_i^{filt}\right\}$, where C_Λ^{filt} and Λ are the outputs of the search algorithm.

Step 6: The set B_i, $i = 1, 2, ..., M$ is searched to obtain the bin centre value, B_Λ (that is, the mean noise value) based on the peak index value obtained in Step 5. The HPA considers B_Λ as the mean noise value.

Step 7: We propose two different methods to compute the descent parameter, β, which serves to differentiate the HPA from the MHPA. The HPA computes β using equation (5), which controls the P_{FA} rate of the detector. In this case, the performance of the HPA can be improved by manually tuning β, however, manual control of β may be impracticable under real-time CR operation in which spectra conditions change per time. Consequently, we have introduced the Mean HPA (MHPA) to compute β as follows:

$$\beta = \frac{1}{2M} \sum_{i=1}^{M} C_i^{filt} \tag{10}$$

The half mean is considered in equation (10) so that β may assume low values required to maintain low P_{FA} rates. The MHPA is motivated knowing that most PDFs often contain more counts in the tail region of the distribution than in other regions. This compels β to assume lower values required to guarantee an autonomous algorithm (such as the MHPA).

Step 8: Both algorithms proceed by initializing a counter, $\rho = \Lambda$, where Λ corresponds to the noise peak index obtained in Step 5. Both algorithms use ρ to search for the minimum point that corresponds to a useful threshold, γ. This process is executed via Steps 9 - 17.

Step 9 - 17: These steps are used to find a useful threshold within B_i, $i = 1, 2, ..., M$. Typically, both algorithms will skip the '*While*' loop in Step 10 if Step 9 returns as false. In this case, it is straightforward to provide an error message to the user. However, Step 10 prevents both algorithms from searching for a useful threshold beyond the M^{th} histogram bin.

Step 12 checks for ρ in C_i^{filt}, while Step 13 obtains the histogram bin θ, that corresponds to ρ. Step 14 then increments M when ρ has been found in Step 13 so that the '*While*' loop is terminated.

Step 18: The threshold is thus obtained as

$$\gamma = B_\theta \tag{11}$$

where B_θ is the bin centre value obtained at the index point, θ.

The process ends here and both algorithms are reinitiated in order to estimate new thresholds for a new set of $Y(k)$ values.

3.3. Time Complexity of the HPA/MHPA

We analyze the time complexity (TC) of both algorithms in this section. The TC is determined based on the number of machine instructions required to execute both algorithms. We have removed all constant factors in order to ensure that the running time is estimated based only on V, particularly as V approaches infinity. Similarly, we have excluded lower order terms to describe the TC asymptotically[38]. Thus, we obtained the asymptotic TC of the HPA and MHPA as follows: Steps 1, 2, 4, 7, 8 and 18 are evaluated once in constant time reducing to steps of $O(1)$. However, steps 5 and 6 are executed in $O(V)$ owing to the search process involved in both steps. Step 3 is executed in $O(MV)$, where M is the number of histogram bins. An effective method, such as the Greedy Batch Dynamic Programming (GDY-BDP) method can be used in step 3 to construct the histogram[37]. Steps 9 to 17 are evaluated in $O(M)$. Based on linearity, the overall TC of both algorithms is obtained as $O(1)+O(V)+O(MV)+O(M) \approx O(MV)$ with $O(MV)$ being the dominant factor. However, because $V >> M$ and neglecting lower order terms, the overall asymptotic TC reduces approximately to $O(V)$. Thus, since both algorithms have an approximate asymptotic TC of $O(V)$, they are considered as fast and highly scalable algorithms much suited for use in CR-IWSNs.

3.4. Empirical Method of Analysis

We analyzed and compared both algorithms and other well-known methods using the empirically estimated probability of detection and the probability of false alarm statistically defined as:

$$P_D = \Pr\left(Y(k) \geq \gamma | H_1\right), \quad k = 1, 2, ..., V \tag{12}$$

$$P_{FA} = \Pr\left(Y(k) < \gamma | H_0\right), \quad k = 1, 2, ..., V \tag{13}$$

The P_D and P_{FA} rates were empirically computed using Fawcett's approach[39]. Following Fawcett's method, the ground truths of the different input signals were obtained and labeled. The ground truths of the simulated signals were obtained by labeling actual signal samples as ones (true signal samples), and noise samples as zeros (true noise samples). The actual thermal noise level of the simulated detector was used as the true threshold to obtain the ground truths. Real-life signals were also used in our experiments. In this case, the corresponding ground truth of each real-life signal set was labeled in similar binary fashion. Here, the maximum true noise value of each dataset was used as the true threshold to classify the ground truth. Thus, the ground truths were all obtained from the true dynamic range of each dataset.

Consequently, the P_D and P_{FA} rates per dataset were computed as[39]:

$$P_D = \frac{\phi}{P} \tag{14}$$

where ϕ is the number of true positives (truly detected signal samples) given that $Y(k) \geq \gamma | H_1$, and P is the total number of actual true signal samples, and

$$P_{FA} = \frac{\varphi}{N_0} \tag{15}$$

where φ is the number of false positives (falsely detected signal samples) given that $Y(k) < \gamma | H_0$, and N_0 is the total number of noise samples. The point performance values of each threshold estimation algorithm were thus obtained from the Receiver Operating Characteristic (ROC) curves plotted per dataset based on the computed P_D and P_{FA} values. These results are tabulated and presented in the result section.

4. Results and Discussion

We present results for the parameter adjustment and testing phase of each algorithm. The *adaptive-only* algorithms considered in our work were fine-tuned using different simulated noise datasets. We considered signal sets obtainable within typical CR based IWSN applications, for example, IWSNs in the proposed TV whitespace for CR[40]. We have described the experimental setup considered to test and analyze the performance of our algorithms. We evaluated each algorithm using both Orthogonal Frequency Division Multiplexing (OFDM) and Frequency Modulated (FM) signals to determine their minimum detectable SNR level. We compared our methods with global-based methods, which are fined tuned by adjusting only two or fewer parameters. We then kept the parameter values of each *adaptive-only* algorithm fixed in the testing phase in order to investigate their respective performances under real-life use-cases. All results obtained are discussed relative to the specifications of the IEEE 802.22 standard for CR, which states that $P_D > 90$ % and $P_{FA} < 10$ %[21].

Table 2. False Alarm Rate under different Noise Uncertainty Levels.

False Alarm Rate, P_{FA} (%)						
	adaptive-only methods			Autonomous methods		
Noise (dB)	**ROHT**[24]	**FOST**[25]	**HPA (Proposed)**	**Otsu**[24]	**MOA**[20]	**MHPA (Proposed)**
0	4.9	9.6	**2.6**	56.0	4.9	9.6
1	3.8	6.8	**2.0**	53.9	3.8	6.8
2	4.2	6.7	**1.5**	56.1	6.7	9.3
3	**0.4**	2.8	2.8	63.3	43.9	2.8
4	3.5	5.9	**1.8**	54.5	42.3	3.5
5	4.0	5.5	**2.9**	53.4	48.3	5.5

4.1. Parameter adjustment phase

The parameters of the HPA and other *adaptive-only* algorithms were adjusted following a Monte Carlo simulation (using 1000 trials) of AWGN samples. We considered Monte Carlo simulations in order to fine-tune accurately and configure each algorithm's parameters ahead of their use under real-time conditions. The average performance of the HPA is presented in Figure 2 under different noise levels as a function of different smoothing window sizes, ω. Our findings indicate that irrespective of the noise level in the band, a smoothing window size of $\omega = 11$ may be sufficient to maintain a minimum steady P_{FA} rate (see Figure 2). Interestingly, a lower window size of $\omega \geq 5$ for the HPA produced also no significant reduction in the algorithm's P_{FA} rate. Nevertheless, we have noted that an exception existed at the $-70dBm$ noise level where the P_{FA} increased for $\omega = 9$ and 10, respectively. These outliers occurred because during the simulation process a number of spurious noise samples typically crossed the threshold value. However, on the average, since $\omega = 5$ produced similar results to $\omega = 11$, we have noted that systems plagued by smaller memory sizes may use $\omega = 5$ to run the HPA, while systems with larger memory sizes may use $\omega = 11$. Nevertheless, irrespective of whether $\omega = 5$ or 11 is used to run the HPA, our findings have indicated that there may be no further improvement in the P_{FA} rate of the HPA above $\omega = 11$. Thus, the use of larger window sizes (i.e. $\omega > 11$) may simply be an inefficient use of system memory, which may not be suited for memory-constrained CR-sensor nodes. Thus, the use of $\omega = 5$ to run the HPA is a better configuration for memory-constrained sensor nodes, which further highlights one of the advantages of the HPA. Nevertheless, we note that the empirical values stated here for ω are valid for the HPA mainly under the assumption of the AWGN model.

Furthermore, the descent parameter β of the HPA was computed for $P_{FA} = 10\%$, which conforms to the IEEE 802.22 standard. Thus, subsequent results of the HPA reported in this paper were based on the following parameter configuration: $\omega = 5$ and $P_{FA} = 10\%$. The parameter values used for the ROHT algorithm[23,24] following similar Monte Carlo simulation (of 1000 trials) are as follows: the standard deviation coefficient (SDC), z, was $z = 2$, while the error limit, ϵ, was $\epsilon = 0.01$ (we have used the same symbols as in[23,24]). The parameter values of the FOST algorithm were set as $k = 1$ (same symbol as used in[25]). These values were subsequently kept fixed for subsequent experiments in the testing phase as typically expected in real-life scenarios.

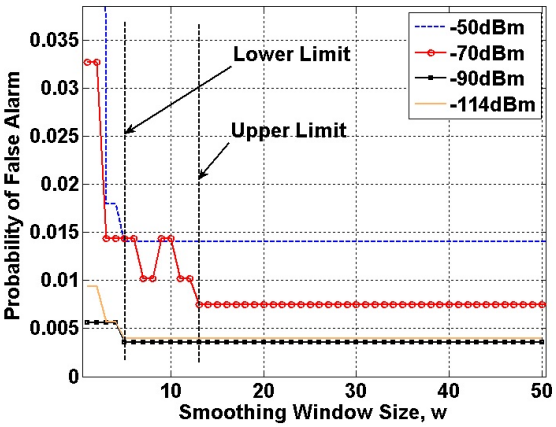

Figure 2. Probability of false alarm for different smoothing factors using the HPA under different noise levels

4.2. Testing phase

The results of the testing phase are based on datasets *unseen* beforehand to each algorithm. This phase models the conditions that most algorithms may typically encounter in real operating CR-IWSN environments. The first subsection presents results for the algorithms tested under different noise uncertainty conditions (noise-only, H_0 case). The subsequent subsections then present results under different signal-plus-noise conditions (H_1 case). Likewise, only P_{FA} rates are presented for the H_0 condition (since PU signals do not exist under the

H_0 condition), while both P_D and P_{FA} rates are reported for the H_1 cases.

4.2.1. Performance under different noise uncertainty levels (H_0 case)

We have investigated the performance of our algorithms under conditions of noise uncertainties. Since this condition may typically confront most CR-based sensors deployed under real-time conditions, thus, we have modeled the case for noise uncertainty by gradually increasing the noise level in steps of 1dB based on a Uniform distribution designed with 1 dB variance on the random open interval (0,1). This uniform 1 dB variance was incrementally added to a baseline thermal noise floor of -106 dBm over a 6 MHz bandwidth, which conforms to the Digital TV band. The P_{FA} of each algorithm estimated per noise uncertainty level is presented in Table 2.

The HPA produced the lowest P_{FA} rate ($P_{FA} < 3\%$) across the entire noise uncertainty range considered in our experiments (see Table 2). This performance was closely followed by the ROHT algorithm[23,24]. The Otsu algorithm produced the highest P_{FA}, thus considered to be the least performer (see Table 2). The Modified Otsu Algorithm (MOA) only performed well at noise uncertainty levels below 3dB, above which a 40 % increase in its P_{FA} rate was recorded. The Otsu and MOA may have performed poorly because they both lacked an effective mechanism to detect accurately the presence of noise-only conditions under unknown spectral measurements. On the other hand, since the parameters of the ROHT, FOST and the HPA were pre-adjusted based on similar AWGN samples (in Section 4.1), their better performance over the autonomous methods (Otsu, MOA and MHPA) is typically expected. However, by being without any form of pre-adjustment, the performance of our proposed MHPA satisfies the stringent requirements of the IEEE 802.22 standard. Since CR-based sensors are typically self-configuring, this finding suggests that our MHPA may be better suited for deployment in CR-IWSN sensors than the other autonomous methods (i.e. Otsu and MOA) considered in our tests. Summarily, our findings have suggested that under the noise uncertainty use-case, our HPA provides the best performance (lowest P_{FA}), while the MHPA performs best under the category of the autonomous methods.

4.2.2. Minimum detectable SNR level (H_1 case)

This section presents our findings per algorithm concerning the use of Orthogonal Frequency Division Multiplexing (OFDM) and Frequency Modulated (FM) signals. The OFDM use-case was considered to model the detection of Digital TV (DTV) signals in CR-IWSNs, while the FM use-case was considered for the case of detecting microphone signals, both of which exist in the TV whitespace intended for CR-IWSN applications. The SNR for both use-cases was varied in order to determine the minimum detectable SNR level of each algorithm. The results obtained are presented in Table 3 and discussed in the next subsections.

Under OFDM signals

For results concerning OFDM signals (see the OFDM column in Table 3), our MHPA achieved a minimum detectable SNR level of $SNR = 4dB$ with ($P_D = 90\%$, $P_{FA} = 3\%$), below which its performance failed to conform to the IEEE 802.22 standard. Other autonomous methods such as the Otsu and MOA provided $P_D = 91\%$, at $SNR = 3dB$, albeit $P_{FA} = 22\%$, which falls below the required standard. Thus, the minimum detectable SNR of the Otsu and MOA was noted at $SNR = 4dB$, although at a higher P_{FA} rate than the MHPA. For the *adaptive-only* methods, our proposed HPA met the IEEE 802.22 standard at a minimum detectable level of $SNR = 5dB$. Both the ROHT and the FOST algorithms failed in this regard even at $SNR = 10dB$, which is undesirable since the minimum detectable level for DTV signals is considered at $SNR = 15.2dB$[41]. The *adaptive-only* methods performed generally poorer than their autonomous counterparts because OFDM signals exhibit typical noise-like characteristics at the crest of the signal (in the frequency domain). This noise-like characteristics may often bias most *adaptive-only* methods into estimating higher threshold values, which may lead to poorer performances (a problem of concept drift[42]). Thus, our findings indicate that autonomous methods are better threshold estimators over OFDM signals than their *adaptive-only* counterparts with our MHPA offering a particularly balanced P_D, P_{FA} performance.

Under FM signals

Table 3 presents results for the FM use-case (i.e. the case of detecting microphone signals in TV whitespaces). The MHPA achieved a minimum detectable SNR level of $SNR = 5dB$, which was the best obtained performance under the category of autonomous methods. Surprisingly, the MOA met the requirement only at $SNR = 10dB$, while the Otsu algorithm failed even at high SNR levels of $SNR = 10dB$. The Otsu and MOA performed poorly because the FM carrier signal occupied a narrower band as compared to the entire sensed bandwidth. This sparse occupancy characteristic caused more noise samples to be accommodated during the estimation process leading to lower threshold estimates. Thus, though the Otsu algorithm may have produced high P_D rates, nevertheless, it experienced very high P_{FA} rates, which is intolerable by the IEEE 802.22 standard.

Nevertheless, our findings indicate further that the class of *adaptive-only* algorithms performed generally better under

Table 3. Probability of Detection and False Alarm (in %) considering OFDM and FM signals at different SNR Levels.

	(P_D, P_{FA}) **in %**											
	adaptive-only Methods						Autonomous Methods					
SNR (dB)	**ROHT** [24]		**FOST** [25]		**HPA (Proposed)**		**Otsu** [24]		**MOA** [20]		**MHPA**	
	OFDM	**FM**	**OFDM**	**FM**	**OFDM**	**FM**	**OFDM**	**FM**	**OFDM**	**FM**	**OFDM**	**FM**
0	(5,5)	(5,5)	(10,9)	(10,9)	(3,3)	(3,3)	(56,56)	(56,56)	(5,5)	(5,5)	(10,10)	(3,3)
1	(17,3)	(23,5)	(22,5)	(23,5)	(11,1)	(12,3)	(72,43)	(87,56)	(11,1)	(23,5)	(16,3)	(12,3)
2	(22,0)	(51,.4)	(29,1)	(58,7)	(11,0)	(43,2)	(86,36)	(87,48)	(81,28)	(51,4)	(29,1)	(43,2)
3	(29,0)	(77,4)	(36,0)	(80,7)	(11,0)	(73,2)	(88,16)	(91,48)	(91,22)	(69,2)	(29,0)	(73,2)
4	(36,0)	(88,4)	(43,0)	**(94,7)**	(11,0)	(72,2)	**(92,8)**	(100,49)	**(92,8)**	(56,0)	(90,3)	(72,2)
5	(36,0)	**(94,3)**	(51,0)	**(97,6)**	**(91,0)**	**(92,2)**	**((94,1)**	(100,45)	**(94,2)**	(78,0)	**(95,5)**	**(92,2)**
10	(43,0)	**(90,0)**	((65,0)	**(91,1)**	**(96,0)**	**(90,0)**	**(96,0)**	(80,0)	**(96,0)**	**(96,3)**	**(96,2)**	**(90,0)**

FM conditions than under the OFDM use-cases. For example, the ROHT, FOST and HPA algorithms achieved a minimum detectable SNR level of 5, 4, and $5dB$, respectively in the FM use-case (see Table 3). This better performance of the *adaptive-only* methods under the FM use-case may be because the FM carrier signal exhibits a very narrow and *spiky* frequency response, which enables better detection performance even under predominant noise-only conditions. Nevertheless, again we note that our proposed MHPA performed best across both the OFDM and FM use-cases making it best suited for use in critical CR-based IWSN applications.

4.2.3. Performance under Narrowband sensing

The narrowband spectra consisted of PU signals fixed at $SNR = 5dB$ and occupying 90 % of the entire band. In this case, each algorithm achieved $P_{FA} < 0.001\%$, which we typically expected since very low noise samples exist in the sensed band. Consequently, we have reported only the P_D results in Figure 3 . We observed that the ROHT and FOST algorithms achieved very low P_D rates, while our proposed HPA and MPHA achieved $P_D > 90\%$ conforming again to the IEEE 802.22 standard. Similar to well-known observations noted in [25,24], we may as well suggest that the ROHT and FOST algorithms performed poorly because both algorithms considered more signal samples while computing thresholds under highly occupied bands ($\approx$ 90%). This may have led to the estimation of larger threshold values as compared to the HPA and MHPA. On the other hand, the HPA and MHPA outperformed the MOA and the original Otsu algorithm because we have introduced the use of the *descent* parameter to bifurcate effectively the histogram of the signal set.

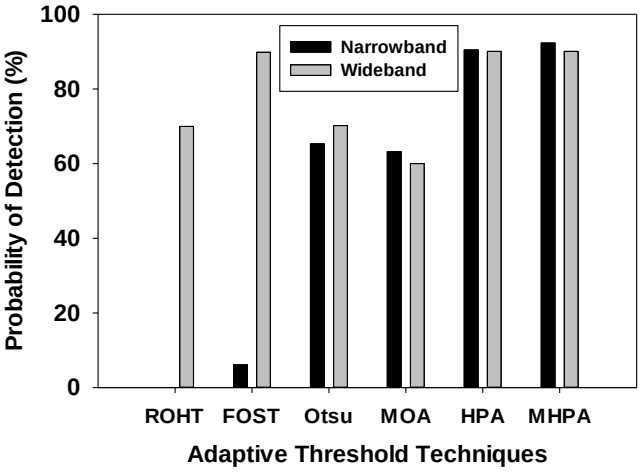

FIGURE 3 Detection performance in both narrow and wide band sensing conditions

4.2.4. Performance under sparse Wideband sensing

A sparsely occupied 50 MHz wideband was sensed in order to test our algorithms based on signals that occupied only 5 MHz of the entire bandwidth ($\approx 8\%$ occupancy rate). We tested each algorithm considering the $SNR = 5dB$ case and results are presented in Figure 3 . In this case, the MOA performed least, while the HPA, MHPA and the FOST algorithm achieved $P_D > 90\%$. Since a larger portion of the sparse band contained more noise samples, this may have reduced the threshold-bias effect experienced by the FOST and ROHT algorithms leading to their better performance under wideband conditions. Nevertheless, again we have observed that our HPA and MHPA performed best under wideband conditions since they depend only on the histogram of the signal set rather than the signal

itself as other techniques may typically do. By processing the histogram of the signal set instead of the signal itself, our HPA and MHPA algorithms are made to be insensitive to the size of bandwidth being sensed, thus making them highly suited for use under both narrow and wideband conditions.

4.3. Performance Evaluation under a typical CR-IWSN Experimental Testbed

We tested each algorithm using real-life signals acquired from emissions in our local TV and FM bands. This use-cases may occur typically under CR-IWSNs conditions particularly in cases where sensor nodes are deployed to operate in the lower VHF and UHF bands within industrial environments. To achieve this, we acquired signals using a Rigol DSA1030

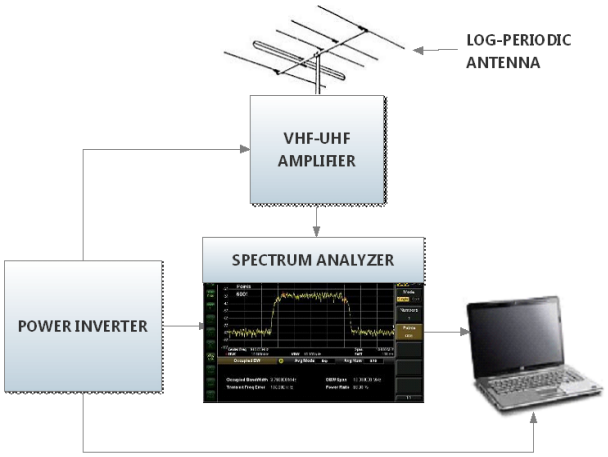

Figure 4. Schematic of the experimental setup used to test and validate the proposed algorithms

spectrum analyzer with the true frequency locations of each PU signal emitted in the local environment been identified via the National frequency allocation table. The schematic of our experimental setup is as shown in Figure 4. In our experimental model, the spectrum analyzer and input antenna are considered to be the frontend of the CR-based sensor node, while our algorithms running within the laptop constitute the processing unit of the sensor node. Our testbed involved the use of a Rigol DSA1030 spectrum analyzer having a frequency range from 9 kHz to 3 GHz. The analyzer has a resolution bandwidth (RBW) range of 100 Hz to 1 MHz, in 1-3-10 sequence, and a video bandwidth (VBW) range of 1 Hz to 3 MHz. Using a RBW of 100Hz, a VBW of 10 Hz, an average detector, and a trace average ≥ 50, we experimented with the Preamplifier of the analyzer kept on along with an average RMS trace detector and a dBm scale unit. The input of the analyzer was coupled to a VHF/UHF broadband TV Log Periodic antenna as shown in Figure 4 having an inbuilt low noise amplifier. Specifically, we used an SAS-510-2 Log Periodic antenna by A.H. Systems Incorporated in our testbed. The antenna provided an input frequency range from 290 MHz to 2 GHz, covering the entire VHF/UHF band being considered for TV whitespace as in CR-IWSN environments. In addition, the antenna provided an antenna factor of 14 - 32 dB and a Gain of 6.5 dBi (specified in the manufacturer's datasheet). This antenna was considered for its excellent cross-polarization property, which greatly reduced the level of measurement uncertainty. Because it is constructed from lightweight aluminium and also directional, we found it suitable for our experimental exercise to ensure that maximum signal gain was achieved. Summarily, a resolution/video bandwidth of 100 Hz was used with a sweep time ranging from 300 - 900 seconds per band. An average detector was used with an attenuation of 0 dB over a single sweep mode. Our experimental setup was deployed in an industrial workshop mimicking the presence of sensors deployed within the environment to sense and communicate over the network. The signal values acquired from our experimental testbed were Power spectra Density (PSD) measurements expressed in dBm/Hz. These acquired real-life PSD samples were saved in Comma Separated Value (CSV) format. Then the CSV formatted datasets were inputted to each algorithm in order to estimate effective thresholds. The results obtained are discussed in the following subsections:

4.3.1. Considering Real-life FM Radio signals

A sample of the acquired FM Radio spectra showing the estimated thresholds by each algorithm is shown in Figure 5. The noise floor slowly ramps upward from left to right of the spectra, thus creating a worthwhile challenge to test our algorithms. The signal (shown in Figure 5) contains 900 samples

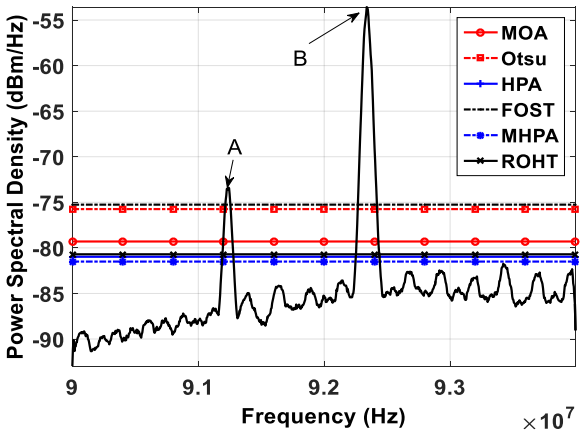

Figure 5. Real FM radio spectrum along with the different thresholds estimated by the different algorithms

acquired between 90 to 94 MHz. Two local FM radio stations were located at 91.2 and 92.3 MHz, respectively. The samples were averaged based on a window size of 10 samples in order to reduce the noise level to enhance each algorithm's performance. Following the noise peak of -81.5 dBm/Hz, station A at 91.2 MHz provided a dynamic range of 7.91 dB, while station B at 92.3 MHz provided a dynamic range of 27.92 dB. Considering both signals being in the same spectra provided a 20 dB difference between the dynamic ranges of both stations, thus further creating a worthwhile challenge for our threshold estimators. Each algorithm was then tested and the results obtained are presented in Table 4 under the FM column.

Since $P_{FA} < 0.001\%$ was obtained for each algorithm (see all thresholds being above the noise floor at -81.5 dBm/Hz), we report only the P_D rates. Our MHPA again achieved the highest P_D rate followed by the HPA algorithm. The FOST algorithm performed least. Consequently, our findings suggest that MHPA is considered highly viable in real cases of unseen real-life datasets. The success of our MHPA further strengthens the case to use autonomous threshold estimators in CR-IWSN applications.

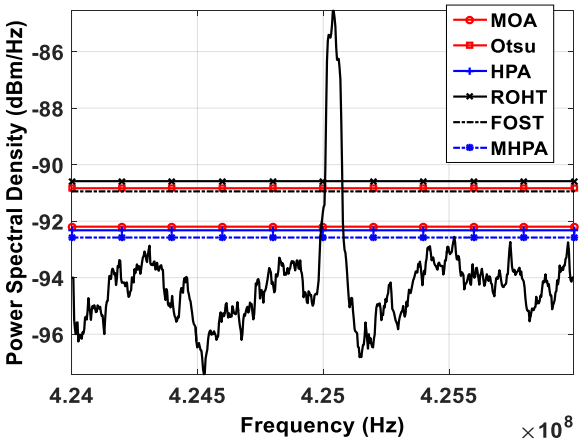

FIGURE 6 Real TV spectrum showing the different thresholds estimated by the different algorithms

4.3.2 Considering Real-life TV signals

Each algorithm was tested using signals measured from a local TV band. The spectra was swept between 424 to 426 MHz using the same Rigol spectrum analyzer described in Section 4.3. A local TV station was sensed with its pilot signal located at 425 MHz (see Figure 6). The spectral samples ($\approx$ 601 samples) were averaged using a window size of 10 samples in order to reduce the noise level in the band. Each algorithm recorded $P_{FA} < 0.001\%$, which can be easily observed following the fact that each respective threshold value laid notably above the noise level (see Figure 6). Consequently, only P_D results are reported in Table 4 under the TV column. From Table 4, the MHPA again provides the best performance as compared to the other methods. The HPA follows in performance terms accompanied by the MOA. The ROHT, FOST and the Otsu algorithm provided similar results in this case. It is suggested that the ROHT and FOST algorithms performed poorly because they depend only on the mean and standard deviation of the dataset, which may be often insufficient to describe fully the underlying properties of the sample distribution. By tracing the entire histogram as considered in our HPA and MHPA, our methods are made more effective than the other methods under the TV signal condition investigated in this section.

5. Conclusion

Two adaptive threshold estimation algorithms, namely the Histogram Partitioning Algorithm (HPA), and the Mean based HPA (MHPA) have been presented to improve threshold estimation in energy detection based Cognitive Radio (CR) Industrial Wireless Sensor Networks (IWSNs). We have compared our new algorithms with some notable threshold estimators under both simulated and real-life signal conditions. From the results obtained, the MHPA (being a fully autonomous algorithm) relatively outperformed other tested methods under different spectra conditions. Our findings reveal that the MHPA estimates effective threshold values automatically at a minimum SNR level of $SNR = 4dB$. Furthermore, both proposed algorithms are notably invariant to the size of the sensed band, thus making them suited for both narrow and wideband sensing in CR-IWSNs. Our algorithms have also a time complexity of $O(V)$, where V is the total number of samples, hence they are considered as quick and highly scalable algorithms suited for CR-based IWSN applications. Nevertheless, the performance of both algorithms can be improved particularly under lower SNR regimes, a condition we shall investigate further in future works.

Appendix

Equation (3) in the main text is derived in this section. Let the FFT length, V, be denoted as

$$V = 2^x, \tag{1}$$

Table 4. Estimated Threshold values and corresponding Probability of considering Real-life FM and TV signals .

Class	Algorithms	Threshold (dBm/Hz)		P_D (%)	
		FM	TV	FM	TV
adaptive-only **Methods**	**ROHT**[24]	-80.70	-90.58	89.71	72.41
	FOST[25]	-75.26	-90.95	63.24	72.41
	HPA	-80.98	-92.32	91.18	93.10
Autonomous Methods	**Otsu**[24]	-75.75	-90.84	67.65	72.41
	MOA[20]	-79.30	-92.20	82.35	89.66
	MHPA	-81.50	-92.57	95.59	96.55

where x is the next power of 2 to be computed. Thus, it is required that

$$2^x > N - 1, \tag{2}$$

where N is the original time domain signal length, which is obtained as $N = T * f_S$, where T is the sensing period, and f_S is the sampling frequency. Note that the number of FFT points goes from $0, 1, ..., N-1$, thus accounting for the use of $N-1$ in equation (2). Thus, from equation (2), x is obtained as

$$x > \log_2(T f_S - 1) \tag{3}$$

By putting equation (3) into (1), the new FFT length is obtained as

$$V = 2^{\lceil \log_2(T f_S - 1) \rceil} \tag{4}$$

The ceiling notation is introduced in equation (4) to guarantee that $x > \log_2(T f_S - 1)$.

References

1. Queiroz DV, Alencar MS, Gomes RD, Fonseca IE, Benavente-Peces C. Survey and systematic mapping of industrial Wireless Sensor Networks. *Journal of Network and Computer Applications* 2017.

2. Oyewobi SS, Hancke GP. A survey of cognitive radio handoff schemes, challenges and issues for industrial wireless sensor networks (CR-IWSN). *Journal of Network and Computer Applications* 2017; 97(July): 140–156. doi: 10.1016/j.jnca.2017.08.016

3. Saad A, Mansour N, Friedrich A, et al. Cognitive radio prototype for industrial applications. *Proceedings of the 22th European Wireless Conference 2016* 2016: 1-8.

4. Akpakwu GA, Silva BJ, Hancke GP, Abu-Mahfouz AM. A Survey on 5G Networks for the Internet of Things: Communication Technologies and Challenges. *IEEE Access* 2017; 3536(c). doi: 10.1109/ACCESS.2017.2779844

5. Järvinen T, Lorite GS, Rautio AR, et al. Portable cyber-physical system for indoor and outdoor gas sensing. *Sensors and Actuators, B: Chemical* 2017; 252: 983–990. doi: 10.1016/j.snb.2017.06.102

6. Chiwewe TM, Mbuya CF, Hancke GP. Using Cognitive Radio for Interference-Resistant Industrial Wireless Sensor Networks: An Overview. *IEEE Transactions on Industrial Informatics* 2015; 11(6): 1466–1481.

7. Ogbodo EU, Dorrell D, Abu-Mahfouz AM. Cognitive Radio Based Sensor Network in Smart Grid: Architectures, Applications and Communication Technologies. *IEEE Access* 2017; 5(c): 19084–19098. doi: 10.1109/ACCESS.2017.2749415

8. Kobo HI, Abu-Mahfouz AM, Hancke GP. A Survey on Software-Defined Wireless Sensor Networks: Challenges and Design Requirements. *IEEE Access* 2017; 5: 1872–1899.

9. Cheng B, Cui L, Jia W, Zhao W, Gerhard PH. Multiple region of interest coverage in camera sensor networks for tele-intensive care units. *IEEE Transactions on Industrial Informatics* 2016; 12(6): 2331–2341.

10. Ozger M, Cetinkaya O, Akan OB. Energy Harvesting Cognitive Radio Networking for IoT-enabled Smart Grid. *Mobile Networks and Applications* 2018; 23(4): 956–966.

11. Silva B, Hancke GP. IR-UWB-based non-line-of-sight identification in harsh environments: Principles and challenges. *IEEE Transactions on Industrial Informatics* 2016; 12(3): 1188–1195.

12. Barnes SD, Maharaj BT. Prediction based channel allocation performance for cognitive radio. *AEU - International Journal of Electronics and Communications* 2014; 68(4): 336–345. doi: 10.1016/j.aeue.2013.09.009

13. Ntshabele K, Isong B, Abu-Mahfouz AM. Analysis of energy inefficiency challenges in cognitive radio sensor network. *in the 44th Annual Conference of the IEEE Industrial Electronic Society* 2018.

14. Wasonga F, Olwal TO, Abu-Mahfouz AM. Efficient two stage spectrum sensing combination for cognitive radio. *In proceedings of the 27th International Symposium on Industrial Electronics (ISIE)* 2018: 1308-1313.

15. Akyildiz IF, Lee WY, Vuran MC, Mohanty S. NeXt generation/dynamic spectrum access/cognitive radio wireless networks: A survey. *Computer Networks* 2006; 50: 2127–2159. doi: 10.1016/j.comnet.2006.05.001

16. Yucek T, Arslan H. A survey of spectrum sensing algorithms for cognitive radio applications. *IEEE communications surveys & tutorials* 2009; 11(1): 116–130. doi: 10.1109/surv.2009.090109

17. Onumanyi AJ, Onwuka EN, Aibinu AM, Ugweje OC, Salami MJE. A real valued neural network based autoregressive energy detector for cognitive radio application. *International Scholarly Research Notices* 2014; 2014: 1–11. doi: 10.1155/2014/579125

18. Onumanyi AJ, Onwuka EN, Aibinu AM, Ugweje O, Salami MJE. Effect of Spectrum Occupancy on the Performance of a Real Valued Neural Networl Based Energy Detector. *International Joint Conference on Neural Networks (IJCNN)* 2014: 1191–1196.

19. Alberti AM, Mazzer D, Bontempo MM, Oliveira dLH, da Rosa Righi R, Cerqueira Sodré A. Cognitive radio in the context of internet of things using a novel future internet architecture called NovaGenesis. *Computers and Electrical Engineering* 2017; 57: 147–161. doi: 10.1016/j.compeleceng.2016.07.008

20. Onumanyi AJ, Onwuka EN, Aibinu AM, Ugweje OC, Salami MJE. A modified Otsu's algorithm for improving the performance of the energy detector in cognitive radio. *AEU-International Journal of Electronics and Communications* 2017; 79: 53–63. doi: 10.1016/j.aeue.2017.04.013

21. IEEE802.22 . Enabling Broadband Wireless Access using Cognitive Radio Technology and Spectrum Sharing in White Spaces. *IEEE 802.22 Working Group on Wireless Regional Area Networks* 2011.

22. Onumanyi AJ, Abu-Mahfouz AM, Hancke GP. A comparative analysis of local and global adaptive threshold estimation techniques for energy detection in cognitive radio. *Physical Communication* 2018; 29(C): 1-11. doi: https://doi.org/10.1016/j.phycom.2018.04.008

23. Datla D, Wyglinski AM, Minden GJ. A Statistical Approach to Spectrum Measurement Processing. *Information and TelecommunicationsTechnology* 2007.

24. Datla D, Wyglinski AM, Minden G. A spectrum surveying framework for dynamic spectrum access networks. *IEEE Transactions on Vehicular Technology* 2009; 58(8): 4158–4168.

25. Gorcin A, Qaraqe KA, Celebi H, Arslan H. An adaptive threshold method for spectrum sensing in multi-channel cognitive radio networks. *17th IEEE International Conference on Telecommunications (ICT)* 2010: 425–429. doi: 10.1109/ictel.2010.5478783

26. Barnes SD, Van Vuuren PJ, Maharaj BT. Spectrum occupancy investigation: Measurements in South Africa. *Measurement* 2013; 46(9): 3098–3112.

27. Vartiainen J, Vuohtoniemi R, Taparugssanagorn A, Promsuk N. Interference Suppression and Signal Detection for LTE and WLAN Signals in Cognitive Radio Applications. *International Journal on Advances in Telecommunications* 2017; 10(1-2): 1-10.

28. Dubey RK, Verma G. Improved spectrum sensing for cognitive radio based on adaptive double threshold. *International Journal of Emerging Trends in Electrical and Electronics (IJETEE)* 2015; 11(2): 1–6.

29. Avila J, Thenmozhi K. Adaptive Double Threshold with Multiple Energy Detection Technique in Cognitive Radio. *Research Journal of Applied Sciences, Engineering and Technology* 2015; 10(11): 1336–1342.

30. Bagwari A, Tomar GS. Two-stage detectors with multiple energy detectors and adaptive double threshold in cognitive radio networks. *International Journal of Distributed Sensor Networks* 2013; 2013.

31. Malafaia D, Vieira J, Tomé A. Adaptive threshold spectrum sensing based on Expectation Maximization algorithm. *Physical Communication* 2016; 21: 60–69. doi: 10.1016/j.phycom.2016.10.004

32. Wang N, Gao Y, Cuthbert L. Spectrum sensing using adaptive threshold based energy detection for OFDM signals. *IEEE International Conference on Communication Systems (ICCS)* 2014: 359–363.

33. Singh A, Bhatnagar MR, Mallik RK. Threshold optimization of a finite sample-based cognitive radio network using energy detector. *EURASIP Journal on Wireless Communications and Networking* 2013; 2013(1): 165.

34. Richardson A. Nonparametric Statistics for Non-Statisticians: A Step-by-Step Approach by Gregory W. Corder, Dale I. Foreman. *International Statistical Review* 2010; 78(3): 451–452.

35. Lehtomaki JJ, Vuohtoniemi R, Umebayashi K. On the measurement of duty cycle and channel occupancy rate. *IEEE Journal on Selected Areas in Communications* 2013; 31(11): 2555–2565. doi: 10.1109/jsac.2013.131114

36. Doane DP. Aesthetic frequency classifications. *The American Statistician* 1976; 30(4): 181–183.

37. Halim F, Karras P, Yap RHC. Fast and effective histogram construction. *Proceedings of the 18th ACM conference on Information and knowledge management* 2009: 1167–1176.

38. Thanh VH, Zunino R, Priami C. Efficient constant-time complexity algorithm for stochastic simulation of large reaction networks. *IEEE/ACM Transactions on Computational Biology and Bioinformatics (TCBB)* 2017; 14(3): 657–667.

39. Fawcett T. An introduction to ROC analysis. *Pattern recognition letters* 2006; 27(8): 861–874.

40. Chandra R, Moscibroda T, Murty RN, Bahl P. Spectrum assignment for networks over white spaces and other portions of the spectrum. 2017. US Patent 9,730,186.

41. Xiao X. Low-Power Spectrum Sensing for Cognitive Radio Applications. Master's thesis. University of California at Berkeley. 2012.

42. Žliobaitė I, Pechenizkiy M, Gama J. An overview of concept drift applications. In: Springer. 2016 (pp. 91–114).